The Visible Absorption Spectrum of $^{16}OBr^{16}O$ and $^{18}OBr^{18}O$ Isolated in Solid Ne

Yu-Chang Lee and Yuan-Pern Lee*

Department of Chemistry, National Tsing Hua University, 101, Section 2, Kuang Fu Road, Hsinchu, Taiwan 30013

Received: February 9, 2000; In Final Form: May 2, 2000

The visible absorption spectrum of OBrO isolated in solid Ne is recorded in the 15 800−20 500 cm^{-1} region. Unlike that reported previously for OBrO in solid Ar, the spectrum in solid Ne has sharp zero-phonon lines (ZPL) exhibiting short progressions of bending (ν_2') mode built upon a long progression of symmetric stretching (ν_1') mode. Use of ^{18}O isotopic labeling resolves discrepancies in vibrational assignments proposed previously. Fitting of the wavenumbers of ZPL yields $T_0 = 15\,818.4 \pm 0.2$, $\omega_1' = 642.77 \pm 0.13$, $\omega_2' = 223.21 \pm 0.43$, $x_{11}' = -2.85 \pm 0.01$, $x_{22}' = -1.07 \pm 0.13$, and $x_{12}' = -2.49 \pm 0.04$ cm^{-1} for the $C^2A_2 \leftarrow X^2B_1$ transition of $^{16}O^{79}Br^{16}O$ and $T_0 = 15\,832.0 \pm 0.2$, $\omega_1' = 612.49 \pm 0.12$, $\omega_2' = 214.01 \pm 0.39$, $x_{11}' = -2.61 \pm 0.01$, $x_{22}' = -1.28 \pm 0.12$, and $x_{12}' = -2.63 \pm 0.04$ cm^{-1} for $^{18}O^{79}Br^{18}O$. A weak line at 16744.3 cm^{-1} may be assigned as 3_0^2 to yield $2\nu_3 = 925.7$ cm^{-1} for $^{16}O^{79}Br^{16}O$. Observed spectral parameters agree well with high-level theoretical predictions by Peterson.

I. Introduction

The role of ClO_x catalytic cycles leading to destruction of ozone in the stratosphere is well established.[1−4] Laboratory studies demonstrate that BrO_x compounds also participate in analogous catalytic cycles. Although much less abundant than ClO_x, BrO_x compounds are more reactive toward destruction of ozone.[5,6] Among possible bromo compounds in the atmosphere, only BrO and HBr are well characterized.[7,8] The observation of OBrO in photodissociation of ozone with sensitized bromine indicates the potential importance of higher bromine oxides in atmospheric chemistry.[9−11] Recently, possible detection of OBrO in the stratosphere indicates that OBrO might be the principal bromine species at night in the middle stratosphere.[12]

Spectral information about OBrO is rather limited. The first unambiguous identification of OBrO was made by Tevault et al.[13] with the matrix isolation/IR absorption technique. Laboratory detection of OBrO in the gas phase was later reported by Butkovskaya et al.[14] Recently, rotational spectra and molecular properties of OBrO X^2B_1 in (000), (010), (020), and (001) states were analyzed;[15,16] reported vibrational wavenumbers of OBrO in the gas phase ($\nu_1 = 799.4$, $\nu_2 = 317.5$, and $\nu_3 = 848.6$ cm^{-1}) are in agreement with those observed in matrices.[13,17,18]

Electronically excited states of OBrO are less well characterized. Rattigan et al.[9] recorded a visible absorption spectrum of OBrO in the 400−600 nm region and suggested that $T_0 = 16\,509$ cm^{-1}, $\omega_1' = 638$ cm^{-1}, and $\omega_2' = 200$ cm^{-1} for the transition. Kölm et al.[18] recorded a spectrum of OBrO isolated in solid Ar that appears similar to that in the gas phase and reported $T_0 = 16\,785 \pm 20$ cm^{-1}, $\omega_1' = 631$ cm^{-1}, and $\omega_2' = 221$ cm^{-1}. Although they also performed experiments on $^{18}OBr^{18}O$, the broad bandwidths precluded unambiguous vibrational assignment of observed progressions. Recently Miller et al.[19] recorded an absorption spectrum of gaseous $^{16}OBr^{16}O$ with improved sensitivity and reported a lower value of $T_0 = 15\,863 \pm 3$ cm^{-1} with $\omega_1' = 641.5$ and $\omega_2' = 210.7$ cm^{-1}. The origin of the transition is thus still uncertain.

A few quantum-chemical calculations are reported for OBrO. Pacios and Gomez[20] employed the second-order unrestricted Møller−Plesset (UMP2) and the coupled cluster with single, double, and noniterative triple excitation (CCSD(T)) methods to obtain the geometry and harmonic vibrational frequencies of OBrO and BrOO; they also calculated possible dissociation asymptotes of both species. Miller et al.[19] reported, in addition to the geometry and harmonic vibrational frequencies of the ground state, geometries and relative energies of three low-lying doublet excited states: A^2B_2, B^2A_1, and C^2A_2. Based on a Franck−Condon simulation and their ab initio calculations, they assigned the observed visible absorption spectrum to the $C^2A_2 \leftarrow X^2B_1$ transition. The most extensive calculation on the C^2A_2 state of OBrO is reported by Peterson,[21] who employed internally contracted multireference configuration interaction coupled with a multireference analogue of the Davidson correction (denoted as icMRCI+Q) to characterize potential energy surface and dipole moment functions near the equilibrium geometry of the X^2B_1 and C^2A_2 states of OBrO and OClO. The analytical potential-energy functions were used to predict anharmonic parameters and vibrational spectra for both electronic states; agreement with available experimental data is satisfactory.

We have previously recorded visible absorption and laser-induced fluorescence spectra of OClO isolated in solid Ne, Ar, and Kr to determine accurate spectral parameters of the $A^2A_2 \rightarrow X^2B_1$ transition.[22] Vibrationally unrelaxed emission from the $A(v \geq 1)$ state was also observed. An absorption continuum underlying the A−X system is tentatively attributed to absorption to the $^2A_1$ state above the predissociation barrier. Site selectivity, mode specificity, and effects of matrix hosts on photolysis of OClO were investigated in detail.[23] Considering that measurements of sharp zero-phonon lines (ZPL) of distinct isotopomers isolated in a Ne matrix might assist to decipher the origin of the OBrO visible absorption, we produced OBrO

* To whom correspondence should be addressed. Jointly appointed by the Institute of Atomic and Molecular Sciences, Academia Sinica, Taipei, Taiwan. E-mail: yplee@mx.nthu.edu.tw.

10.1021/jp000527y CCC: $19.00
Published on Web 07/08/2000

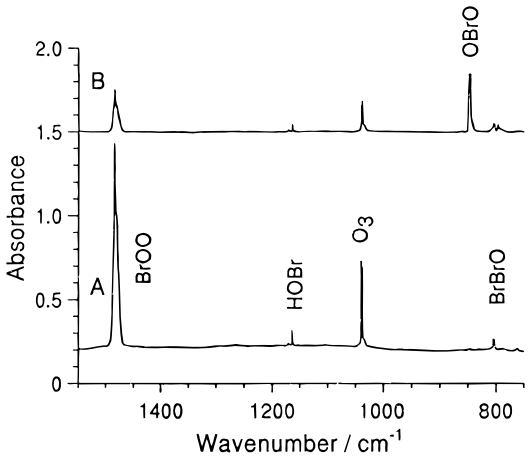

Figure 1. Partial IR absorption spectra of the matrix sample before and after laser irradiation. (A) After deposition of ~16 mmol of discharged Br_2/O_2/Ne (1/5/2000) for 1 h; (B) after irradiation of the matrix at 248 nm for 20 min.

in solid Ne with a photochemical method and recorded visible absorption spectra with a Fourier transform spectrometer. Accurate determination of line positions of both $^{16}OBr^{16}O$ and $^{18}OBr^{18}O$ leads to unambiguous vibrational assignments and improved spectral parameters.

II. Experiments

The experimental setup is similar to that described previously.[22] The system is designed so that absorption spectra extending from the far-infrared to visible regions as well as laser-induced fluorescence spectra may be recorded with the same matrix sample. The matrix support was a platinum-plated copper mirror maintained at 5 K. Matrix samples were prepared on depositing microwave-discharged gas mixtures of Br_2 in Ne (1/2000) and O_2 in Ne (1/400) onto the matrix support. Typically ~6 mmol of mixture was deposited over a period of 1 h. The major product after deposition is BrOO, which is converted to OBrO on irradiation of the matrix with light from a KrF excimer laser at 248 nm (2 mJ, 10 Hz) for ~20 min. UV photoconversion of BrOO to OBrO was monitored with a Fourier transform spectrometer (Bomem DA8.3). IR absorption spectra were recorded with a globar source, a KBr beam splitter, and a HgCdTe detector (77 K). For measurements of near-infrared and visible absorption spectra, we employed a quartz-halogen lamp, a quartz beam splitter, and a photomultiplier to cover the spectral range 11 000−25 000 cm^{-1}. Typically 400 scans were collected at a resolution of 0.5 cm^{-1}.

Br_2 (Across Organics, 99.8%), Ne (AGA Specialty Gases, 99.99%), O_2 (Fulgent Scientific Inc., 99.99%), and $^{18}O_2$ (Matheson, 97% isotopic purity) were used without purification except for degassing of Br_2 at 77 K.

III. Results and Discussion

Miller et al.[19] generated OBrO by flowing Br_2 and a discharged mixture of O_2 in He through an absorption cell maintained at 250 K, followed by pumping on the condensate collected on the wall of the cooled cell. Kölm et al.[18] produced matrix-isolated OBrO by co-deposition of a microwave-discharged mixture of Br_2 in Ar with a mixture of O_2 in Ar onto the sample support, followed by irradiation of the matrix sample with laser light at 280 nm. We found that the yield is better when we passed both O_2 and Br_2 (both diluted in Ne) through a microwave discharge before deposition, followed by irradiation of the matrix sample at 248 nm. Figure 1A shows an IR absorption spectrum in the region 700−1600 cm^{-1} after deposition; it reveals that the matrix contains predominantly BrOO and O_3, with a trace of BrBrO. After irradiation of the matrix sample at 248 nm with a KrF excimer laser (2 mJ with an area ~1 cm^2, 10 Hz) for 20 min, a substantial amount of BrOO is converted to OBrO, as shown in Figure 1B. BrOO and O_3 do not absorb strongly in the region (15 800−20 500 cm^{-1}) of interest; therefore they do not interfere with the absorption spectrum of OBrO. IR absorption lines of OBrO, BrOO, BrBrO, and BrO in solid Ne, not reported previously, are listed in Table 1 for comparison with those in solid Ar[13,18,24] and in the gas phase.[19,25]

TABLE 1: Comparison of IR Absorption Wavenumbers (in cm^{-1}) of Various Isotopomers of Bromine Oxides Isolated in Matrices and in the Gas Phase

species	mode	solid Ne this work	solid Ar	ref	gas	ref
$^{16}O^{79}Br^{16}O$	ν_1	797.6	795.7	18	799.4	19
	ν_2	−	317.0		317.5	
	ν_3	848.4	845.2		848.6	
$^{16}O^{81}Br^{16}O$	ν_1	795.6	794.6	18		
	ν_2	−	316.3			
	ν_3	846.1	842.8			
$^{18}O^{79}Br^{18}O$	ν_1	758.5	756.4	18		
	ν_2	−	302.1			
	ν_3	811.4	808.4			
$^{18}O^{81}Br^{18}O$	ν_1	757.2	755.0	18		
	ν_2	−	301.4			
	ν_3	809.2	806.1			
$^{79}Br^{16}O^{16}O$	ν_1	1487.0	1485.1	18		
$^{79}Br^{18}O^{18}O$	ν_1	1400.7	1402.3	18		
$^{79}Br^{79}Br^{16}O$	ν_3	804.8 (803.3)[a]	804.1	13		
$^{79}Br^{79}Br^{18}O$	ν_3	767.5 (765.7)	767.2	13		
$^{79}Br^{16}O$	ν_1	724.1	729.9	13	723.414 20	25
$^{81}Br^{16}O$	ν_1	722.6			721.927 15	25
$^{79}Br^{18}O$	ν_1	690.1 (688.5)	695.5	13		
$^{79}Br^{16}O^{79}Br$	ν_1	−	526.1	13		
	ν_3	621.4 (620.1)	623.4			
$^{79}Br^{18}O^{79}Br$	ν_3	593.0 (591.6)	592.1	13		

[a] Numbers in parentheses are associated with a minor matrix site.

Figure 2A shows the difference absorption spectrum in the visible region 15 800−20 500 cm^{-1} recorded after photoconversion of BrOO to OBrO. The spectrum consists of progressions with each band containing a set of three sharp lines separated by ~19 and 22 cm^{-1}, presumably corresponding to OBrO in distinct matrix sites, and broad phonon wings. The spectrum exhibits short progressions with spacings 200−220 cm^{-1} built upon a long progression with spacings 576−636 cm^{-1}. The wavenumbers of each line are listed in Table 2 with those associated with two minor sites in parentheses. Based on previous experimental and theoretical results, the two progressions correspond to the bending (ν_2) and symmetric stretching (ν_1) modes of OBrO, respectively.

The $A^2A_2 \leftarrow X^2B_1$ transition of OClO also displays multiple sites in various matrices.[22] In solid Ar and Kr, lines associated with two additional minor sites are separated by ~31, 63 and ~40, 74 cm^{-1}, respectively, from the major peak. However, only one prominent site was observed for OClO in solid Ne.

Isotopically enriched $^{18}OBr^{18}O$ was produced by replacing $^{16}O_2$ with $^{18}O_2$. IR absorption wavenumbers of $^{18}OBr^{18}O$, $Br^{18}O^{18}O$, and $BrBr^{18}O$ in a Ne matrix are also listed in Table 1 for comparison. The visible absorption spectrum of $^{18}OBr^{18}O$ is shown in Figure 2B, with observed line positions listed in Table 2; wavenumbers associated with minor sites are listed in parentheses. Because the ^{18}O isotopic shifts for the ν_1 mode are large (~30 cm^{-1}), vibrational assignments based on isotopic shifts are unambiguous. The assignments, indicated in Figure

TABLE 2: Visible Absorption Wavenumbers (in cm^{-1}) of the $C^2A_2 \leftarrow X^2B_1$ System of $^{16}OBr^{16}O$ and $^{18}OBr^{18}O$ Isolated in Solid Ne

assignment			$^{16}OBr^{16}O$		$^{18}OBr^{18}O$	
v_1'	v_2'	v_3'	expt	o − c[a]	expt	o − c[a]
0	0	0	15 818.60	0.24	15 831.90	−0.12
			(15 838.32, −)[b]	(0.48, −)[b]		
0	1	0	16 038.56	0.38	16 042.28	−0.11
			(16 057.46, 16 076.74)	(0.10, −0.41)		
0	2	0	16 256.10	0.23	−	−
			(16 274.98, 16 292.50)	(−0.30, 0.19)		
1	0	0	16 454.12	−0.08	16 438.02	0.05
			(16 473.80, 16 497.80)	(0.01, 1.16)	(16 458.12, 16 481.83)[b]	(0.01, −0.31)[b]
1	1	0	16 671.12	−0.41	16 645.70	0.21
			(16 690.47, 16 710.55)	(−0.21, −0.63)	(16 664.51, 16 685.81)	(−0.23, 0.31)
0	0	2	16 744.30			
1	2	0	16 886.49	−0.23	16 850.34	−0.12
			(16 906.05, 16 926.09)	(0.07, 2.67)	(16 870.17, 16 886.84)	(0.24, −0.37)
2	0	0	17 084.13	−0.22	17 038.87	0.17
			(17 103.71, 17 127.24)	(−0.43, −0.39)	(17 058.50, 17 083.12)	(0.14, 0.50)
2	1	0	17 298.73	−0.46	17 243.29	−0.30
			(17 318.42, 17 338.12)	(0.01, −1.14)	(17 262.72, 17 283.31)	(0.07, −0.19)
2	2	0	17 511.91	0.03	17 446.21	0.29
			(17 531.06, 17 546.02)	(−0.04, −2.57)	(17 465.49, 17 483.06)	(0.01, 0.34)
3	0	0	17 708.62	−0.18	17 634.11	−0.08
			(17 728.53, 17 752.02)	(−0.36, −0.64)	(17 653.08, 17 677.50)	(−0.44, −0.51)
3	1	0	17 920.99	−0.16	17 836.24	−0.22
			(17 940.62, 17 961.14)	(0.07, 0.24)	(17 855.38, 17 876.40)	(−0.08, 0.01)
3	2	0	18 131.40	−0.04	18 035.69	−0.48
			(18 150.86, 18 167.13)	(0.25, −0.67)	(18 055.89, 18 073.00)	(−0.05, −0.15)
4	0	0	18 327.74	0.17	18 224.28	−0.18
			(18 347.72, 18 371.72)	(−0.33, −0.03)	(18 244.03, 18 268.96)	(0.43, 0.65)
4	1	0	18 537.74	0.31	18 424.20	0.10
			(18 557.38, 18 578.00)	(0.29, 0.45)	(18 443.04, 18 464.79)	(−0.14, 0.56)
4	2	0	18 745.25	0.10	18 621.50	0.32
			(18 764.82, 18 781.98)	(0.28, 0.93)	(18 641.50, 18 658.79)	(0.19, 0.30)
5	0	0	18 940.67	0.02	18 809.70	0.20
			(18 961.83, 18 985.90)	(0.21, 1.03)	(18 828.69, 18 853.08)	(0.10, −0.45)
5	1	0	19 147.97	−0.05	19 006.87	0.36
			(19 167.95, 19 189.55)	(−0.10, 1.79)	(19 026.02, 19 046.20)	(0.21, −0.77)
5	2	0	19 353.34	0.10	19 200.80	−0.17
			(19 372.90, −)	(−0.03, −)	(19 220.70, 19 238.56)	(−0.89, −0.19)
6	0	0	19 548.32	0.29	19 389.09	−0.23
			(19 570.09, 19 591.75)	(−0.50, −0.30)	(19 408.56, 19 433.50)	(0.08, −0.16)
6	1	0	19 753.38	0.47	19 583.79	0.09
			(19 773.47, 19 792.21)	(0.07, 0.19)	(19 603.53, 19 624.70)	(0.17, 0.09)
6	2	0	19 955.39	−0.26	19 775.70	0.17
			(19 975.32, 19 989.14)	(−0.29, −0.56)	(19 797.28, 19 814.00)	(0.50, 0.08)
7	0	0	20 149.97	0.24	19 964.10	0.20
			(20 171.90, 20 192.44)	(−0.08, −0.83)	(19 982.97, 20 008.97)	(−0.32, 0.26)
7	1	0	20 352.04	−0.08	20 155.30	−0.36
			(20 372.94, −)	(−0.23, −)		
8	0	0	20 745.25	−0.49	20 532.8?[c]	
					(−, 20 578.70)	(−, 0.03)
8	1	0			20 723.0?	
9	0	0			21 093.1?	

[a] Observed minus calculated values in cm^{-1}. [b] Lines associated with minor matrix sites are listed in parentheses. [c] Values not included in the fitting due to large uncertainties in measurements.

2 and Table 2, are consistent with those proposed by Miller et al.[19] Assignments by Kölm et al.[18] and by Rattigan et al.[9] are off by one vibrational quantum in ν_1.

The progression corresponding to the major site is fitted with the equation

$$\nu = A + \sum_i \omega_i'\left(v_i' + \frac{1}{2}\right) + \sum_{j\geq i} x_{ij}'\left(v_i' + \frac{1}{2}\right)\left(v_j' + \frac{1}{2}\right) \quad (1)$$

in which A is the potential energy surface minimum of the C^2A_2 state relative to the zero point level of the X^2B_1 state, to yield $T_0 = 15\,818.4 \pm 0.2$, $\omega_1' = 642.77 \pm 0.13$, $\omega_2' = 223.21 \pm 0.43$, $x_{11}' = -2.85 \pm 0.01$, $x_{22}' = -1.07 \pm 0.13$, and $x_{12}' = -2.49 \pm 0.04$ cm^{-1} for $^{16}OBr^{16}O$ and $T_0 = 15\,832.0 \pm 0.2$, $\omega_1' = 612.49 \pm 0.12$, $\omega_2' = 214.01 \pm 0.39$, $x_{11}' = -2.61 \pm 0.01$, $x_{22}' = -1.28 \pm 0.12$, and $x_{12}' = -2.63 \pm 0.04$ cm^{-1} for $^{18}OBr^{18}O$, as summarized in Table 3. Deviations (observed minus calculated values) in wavenumbers for each lines are also listed in Table 2 as "o − c". Observed deviations for most lines are less than 0.5 cm^{-1}, the resolution of our measurements. Similarly, lines corresponding to two minor sites are fitted; deviations are listed in Table 2 (in parentheses) and spectral parameters are listed in Table 3. Measurements of lines and fitted spectral parameters corresponding to the high-frequency sites are less accurate because of greater width and interference from phonon wings.

Spectral parameters reported by various works are compared in Table 4. The observed transition origin for $^{16}O^{79}Br^{16}O$ in

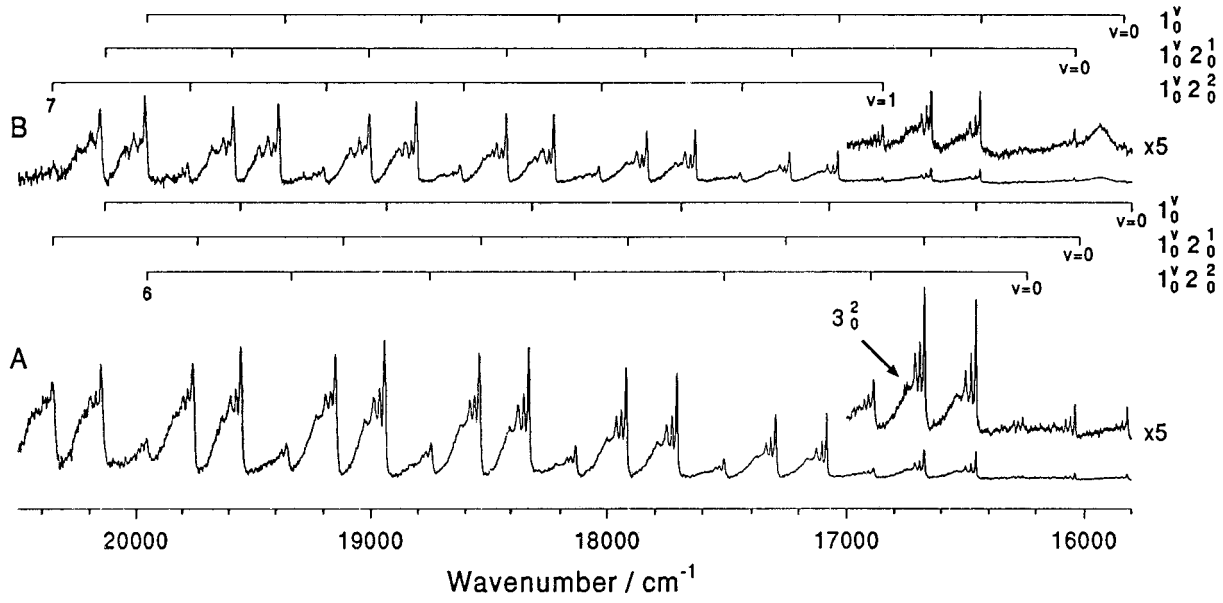

Figure 2. Partial visible absorption spectra of $^{16}OBr^{16}O$ (A) and $^{18}OBr^{18}O$ (B).

TABLE 3: Fitted Spectral Parameters (in cm^{-1}) for $^{16}O^{79}Br^{16}O$ and $^{18}O^{79}Br^{18}O$ Isolated in Various Matrix Sites

	$^{16}O^{79}Br^{16}O$			$^{18}O^{79}Br^{18}O$		
	major site	minor sites		major site	minor sites	
T_0	15 818.4 ± 0.2	15 837.8 ± 0.2	15 859.7 ± 1.4	15 832.0 ± 0.2	15 852.8 ± 0.5	15 876.6 ± 0.5
ω_1'	642.77 (13)[a]	642.84 (13)	644.35 (80)	612.49 (12)	611.61 (28)	611.89 (36)
ω_2'	223.21 (43)	222.42 (43)	221.21(221)	214.01 (39)	211.62 (62)	208.73 (74)
x_{11}'	−2.85 (1)	−2.80 (1)	−2.98 (8)	−2.61 (1)	−2.54 (3)	−2.54 (3)
x_{22}'	−1.07 (13)	−0.80 (13)	−1.15(63)	−1.28 (12)	−0.73 (19)	−0.82 (22)
x_{12}'	−2.49 (4)	−2.62 (4)	−2.91 (20)	−2.63 (4)	−2.35 (6)	−2.48 (7)

[a] The standard deviations of the fitting are listed in parentheses with unit corresponding to the least significant figure.

TABLE 4: Comparison of Spectral Parameters (in cm^{-1}) of the C^2A_2 State of OBrO

	$^{16}OBr^{16}O$					$^{18}OBr^{18}O$	
	this work solid Ne	Miller et al. (ref 19) gas	Rattigan et al. (ref 9) gas	Kölm et al. (ref 18) solid Ar	Peterson (ref 21) calcd	this work solid Ne	Kölm et al. (ref 18) solid Ar
T_0	15 818.6 ± 0.5	15 863 ± 3	16 509[a]	16 785 ± 20[a]	∼16 020	15 831.9 ± 0.5	16 805 ± 20[a]
ν_1'	635.5	636	614		630.4	606.1	
ν_2'	220.0	215	200		208.2	210.4	
$2\nu_3'$	925.7				934.5[b]		
ω_1'	642.77 ± 0.13	641.5	638	631	641.7	612.49 ± 0.12	589
ω_2'	223.21 ± 0.43	210.7	∼200	221	212.8	214.01 ± 0.39	214
ω_3'					446.7		
x_{11}'	−2.85 ± 0.01	−3.52	−3.58		−2.54	−2.61 ± 0.01	
x_{22}'	−1.07 ± 0.13	1.09	−		−0.93	−1.28 ± 0.12	
x_{12}'	−2.49 ± 0.04	−2.70	−		−2.45[c]	−2.63 ± 0.04	

[a] Error in vibrational assignment leads to a greater value of T_0; see text. [b] ν_3' is predicted to be 453.8 cm^{-1} [c] $x_{33}' = 6.85$, $x_{13}' = -10.07$, and $x_{23}' = -3.08$ cm^{-1}.

solid Ne lies at 15 818.6 cm^{-1}, red-shifted by only 45 cm^{-1} from the gas phase. The shift is similar to that (24 cm^{-1}) observed for OClO,[22] indicating that the Ne host perturbs guest molecules only slightly. The ν_1' stretching frequency in Ne (635.5 cm^{-1}) is similar to that in the gas phase (636 cm^{-1}), whereas the ν_2' bending frequency in Ne (220.0 cm^{-1}) is increased by ∼5.0 cm^{-1} (2.3%) from the gas-phase value of 215 cm^{-1}. A similar trend was observed for OClO in Ne, with ν_2' (292.5 cm^{-1}) increased by ∼4.4 cm^{-1} (1.5%) from the gas phase (288.1 cm^{-1}). Compared with the gas-phase values, our values of anharmonicity fit better with theoretical calculations (Table 4) because of improved resolution and line width in this work.

For OClO, absorption lines associated with the asymmetric stretch (ν_3') of the upper state are observed to yield $2\nu_3' = 887.6$ cm^{-1}. Peterson[20] ascribed the atypically large activity of the asymmetric stretch of the $^2A_2$ state of OClO to the strong anharmonic coupling between the two stretching vibrations ($x_{33} = 23.69$ cm^{-1} and $x_{13} = -50.40$ cm^{-1}). According to Peterson, such activity in the ν_3 mode is smaller in OBrO ($x_{33} = 6.85$ cm^{-1} and $x_{13} = -10.07$ cm^{-1}). We searched carefully and found a small peak at 16 744.3 cm^{-1} that may be assigned to the 3_0^2 line of $^{16}O^{79}Br^{16}O$, as marked in Figure 2. The spacing from the origin, 925.7 cm^{-1}, yields $2\nu_3$. This value is consistent with the theoretically predicted value of 934.5 cm^{-1} (with anhar-

monicity taken into account).[21] Unfortunately, the 3_0^2 line of $^{18}O^{79}Br^{18}O$ cannot be positively identified because the weak line is buried in the phonon structures of the $1_0^1 2_0^2$ line.

The A^2B_2 is unlikely to be the upper state of observed absorption because the $A^2B_2 \leftarrow X^2B_1$ transition is electric dipole forbidden, and the energy (12 580 cm^{-1})[19] predicted for the A state is too small in relation to the observed value of T_0. Predicted energies of states B^2A_1 and C^2A_2, 16 335 and 16 760 cm^{-1} respectively, are both similar to observed T_0, but Miller et al.[19] assigned the upper state as C^2A_2 based on calculations of Franck−Condon factors. The observed Franck−Condon distribution requires an increase of Br−O bond length by 0.11 ± 0.01 Å and a decrease of OBrO bond angle by 10.0 ± 0.5° in the excited state, consistent with predicted geometry of the C^2A_2 state ($r = 1.759 \pm 0.010$ Å and $\theta = 104.4 \pm 0.5°$).[19] The Franck−Condon distribution of OBrO observed in solid Ne is similar to that in the gas phase. Such similarity and the small matrix shift indicate that the absorption observed in solid Ne corresponds to the same transition reported in the gas phase.

Although the ν_3' line of $^{18}O^{79}Br^{18}O$ is unobserved, ^{18}O isotopic shifts of ν_1' and ν_2' might still provide an estimate of the bond angle of the upper state based on a simple valence force model. Observed ω_1 and ω_2 values for $^{16}OBr^{16}O$ and $^{18}OBr^{18}O$ were used to solve the equations

$$4\pi^2(\omega_1{}^2 + \omega_2{}^2) = \left(1 + \frac{2m_Y}{m_X}\cos^2\alpha\right)\frac{k_1}{m_Y} + \frac{2}{m_Y}\left(1 + \frac{2m_Y}{m_X}\sin^2\alpha\right)\frac{k_\delta}{l^2} \quad (2)$$

$$16\pi^4\omega_1{}^2\omega_2{}^2 = 2\left(1 + \frac{2m_Y}{m_X}\right)\frac{k_1}{m_Y{}^2}\frac{k_\delta}{l^2} \quad (3)$$

in which m_X and m_Y are masses of Br and O, respectively, and k_1 and k_δ/l^2 are force constants.[26] The bond angle 2α thus derived is 80° ± 20°, favoring C^2A_2 ($2\alpha = 104°$) rather than B^2A_1 ($2\alpha = 118°$) as the upper state. The large error reflects the uncertainty associated with the isotopic ratio in eq 3. If we use $2\alpha = 118°$ in eq 2, we obtain imaginary values of k_1. Hence, we conclude that observed visible spectrum is due to the $C^2A_2 \leftarrow X^2B_1$ transition of OBrO.

We also observed a broad feature starting ~12 000 cm^{-1} with a maximum ~12 600 cm^{-1}. Although the energy is near that predicted for the A^2B_2 state, we exclude this assignment because an identical spectrum was recorded when only discharged Br_2/Ne was present in the system.

We attempted to record laser-induced fluorescence of OBrO by exciting it with laser light at 16 256.1 (2_0^2 line), 16 454.1 (1_0^1 line), and 16 671.1 cm^{-1} ($1_0^1 2_0^1$ line), but the fluorescence was too weak to yield a satisfactory dispersed spectrum. In the case of OClO, weak fluorescence was observed when the low-lying vibronic levels were excited,[21] whereas severe predissociation prevents detection of fluorescence initiating from higher levels. Excitation of OBrO to the low-lying vibronic levels is further limited by small Franck−Condon factors.

Conclusions

We recorded visible absorption spectrum of OBrO isolated in solid Ne in the spectral region 15 800−20 500 cm^{-1}. Observed sharp zero-phonon lines enable us to derive an unambiguous vibrational assignment of the upper state based on ^{18}O isotopic shifts, hence resolving the discrepancies of previous reports. Spectral parameters of the C^2A_2 state are improved, with those for $^{18}OBr^{18}O$ accurately determined for the first time; they are in excellent agreement with recent theoretical calculations.

Acknowledgment. This work is supported by the National Science Council of the Republic of China (Grant No. NSC89-2119-M-007-001).

References and Notes

(1) *Scientific Assessment of Ozone Depletion: 1994, WMO Global Ozone Research and Monitoring Project*; Report No. 37, 1994.
(2) Sander, S. P.; Friedl, R. R.; Francisco, J. S. In *Progress and Problems in Atmospheric Chemistry*; Barker, J. R., Ed.; World Scientific: Singapore, 1995.
(3) Anderson, J. G.; Brune, W. H.; Profitt, M. H. *J. Geophys. Res.* **1989**, *94*, 11465.
(4) Molina, M. J. *Angew. Chem., Int. Ed. Engl.* **1996**, *35*, 1778 and references therein; *Angew. Chem.* **1996**, *108*, 1900.
(5) Sander, S. P.; Watson, R. T. *J. Phys. Chem.* **1981**, *85*, 4000.
(6) Wennberg, P. O.; Cohen, R. C.; Stimpfle, R. M.; Koplow, J. P.; Anderson, J. G.; Salawitch, R. J.; Fahey, D. W.; Woodbridge, E. L.; Keim, E. R.; Gao, R. S.; Webster, C. R.; May, R. D.; Toohey, D. W.; Avallone, L. M.; Profitt, M. H.; Loewnestein, M.; Podolske, J. R.; Chan, K. R.; Woofsy, S. C. *Science* **1994**, *226*, 398.
(7) Scharffler, S. M.; Heidt, L. E.; Pollock, W. H.; Gilpin, T. M.; Vedder, J. F.; Solomon, S.; Lueb, R. A.; Atlas, E. L. *Geophys. Res. Lett.* **1993**, *20*, 2567.
(8) Garcia, R. R.; Solomon, S. *J. Geophys. Res.-Atmos.* **1994**, *99* (D6), 12937.
(9) Rattigan, O. V.; Jones, R. L.; Cox, R. A. *Chem. Phys. Lett.* **1994**, *230*, 121.
(10) Rattigan, O. V.; Cox, R. A.; Jones, R. L. *J. Chem. Soc., Faraday Trans.* **1995**, *91*, 4189.
(11) Rowley, D. M.; Harwood: M. H.; Freshwater, R. A.; Jones, R. L. *J. Phys. Chem.* **1996**, *100*, 3020.
(12) Renard, J.-B.; Pirre, M.; Robert, C. *J. Geophys. Res.* **1998**, *103* (D19), 25383.
(13) Tevault, D. E.; Walker, N.; Smardzewski, R. R.; Fox, W. B. *J. Phys. Chem.* **1978**, *82*, 2733.
(14) Butkovskaya, N. I.; Morozov, I. I.; Tal'rose, V. L.; Vasiliev, E. S. *Chem. Phys.* **1983**, *79*, 21.
(15) Müller, H. S. P.; Miller, C. E.; Cohen, E. A. *Angew. Chem., Int. Ed. Engl.* **1996**, *35*, 2129; *Angew. Chem.* **1996**, *108*, 2285.
(16) Müller, H. S. P.; Miller, C. E.; Cohen, E. A. *J. Chem. Phys.* **1997**, *107*, 8292.
(17) Maier, G.; Bothur, A.; *Z. Anorg. Allg. Chem.* **1995**, *621*, 743.
(18) Kölm, J.; Engdahl, A.; Schrems, O.; Nelander, B. *Chem. Phys.* **1997**, *214*, 313.
(19) Miller, C. E.; Nickolaisen, S. L.; Francisco, J. S.; Sander, S. P. *J. Chem. Phys.* **1997**, *107*, 2300.
(20) Pacios, L. F.; Gómez, P. C. *J. Phys. Chem. A* **1997**, *101*, 1767.
(21) Peterson, K. A. *J. Chem. Phys.* **1998**, *109*, 8864.
(22) Liu, C.-P.; Lai, L.-H.; Lee, Y.-Y.; Hung, S.-C.; Lee, Y.-P. *J. Chem. Phys.* **1998**, *109*, 978.
(23) Lai, L.-H.; Liu, C.-P.; Lee, Y.-P. *J. Chem. Phys.* **1998**, *109*, 988.
(24) Allen, S. D.; Pollakoff, M.; Turner, J. J. *J. Mol. Struct.* **1987**, *157*, 1.
(25) Orlando, J. J.; Burkholder, J. B.; Bopegedera, A. M. R. P.; Howard, C. J. *J. Mol. Spectrosc.* **1991**, *145*, 278.
(26) Herzberg, G. *Molecular Spectra and Molecular Structure, II. Infrared Raman Spectra of Polyatomic Molecules*; van Nostrand Reinhold: New York, 1945.